Accepted Manuscript

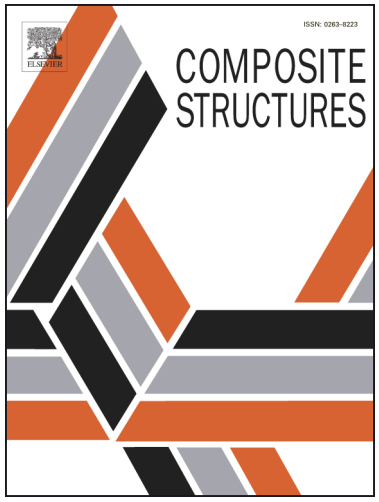

Thermal-mechanical-electrical buckling behavior of functionally graded micro-beams based on modified couple stress theory

X.L. Jia, L.L. Ke, X.L. Zhong, Y. Sun, J. Yang, S. Kitipornchai

PII: S0263-8223(18)30249-6
DOI: https://doi.org/10.1016/j.compstruct.2018.03.025
Reference: COST 9472

To appear in: *Composite Structures*

Received Date: 15 January 2018
Revised Date: 26 February 2018
Accepted Date: 12 March 2018

Please cite this article as: Jia, X.L., Ke, L.L., Zhong, X.L., Sun, Y., Yang, J., Kitipornchai, S., Thermal-mechanical-electrical buckling behavior of functionally graded micro-beams based on modified couple stress theory, *Composite Structures* (2018), doi: https://doi.org/10.1016/j.compstruct.2018.03.025

Thermal-mechanical-electrical buckling behavior of functionally graded micro-beams based on modified couple stress theory

X.L. Jia[1*], L.L. Ke[2*], X.L. Zhong[1], Y. Sun[1], J. Yang [3], S. Kitipornchai[4]

[1] College of Mechanical and Transportation Engineering, China University of Petroleum-Beijing, Beijing, 102249, China

[2] Institute of Engineering Mechanics, Beijing Jiaotong University, Beijing, 100044, China

[3] School of Aerospace, Mechanical and Manufacturing Engineering, RMIT University, PO Box 71, Bundoora, VIC 3083 Australia

[4] School of Civil Engineering, The University of Queensland, Brisbane, St Lucia 4072, Australia

Abstract: This paper presents thermal-mechanical-electrical buckling analysis of micro-beams that are made of functionally graded materials(FGMs) with temperature-dependent thermo-elastic properties. The material properties of the micro-beam are assumed to be graded in the thickness direction according to a simple power law distribution in terms of the volume fractions of the constituents. The governing equations are based on the principle of the minimum total potential energy, von Kármán geometric nonlinearity theory, and modified couple stress theory is employed to consider the size effect. A differential quadrature (DQ) method combined with an iteration process is used to predict the critical buckling external axial force and buckling temperature increment. The effects of the volume fraction profile parameter, dimensionless length scale parameter, initial gap ratio, ground electrode shape parameter, the applied voltage, slenderness ratio and the axial residual stress on the thermal-mechanical-electrical buckling behavior are evaluated in detail through parametric studies.

Keywords: Functionally graded materials; Micro-beam; Size effect; Thermal-mechanical-electrical buckling

Corresponding author, Tel: +86 10 89733762, E-mail address: xljia@cup.edu.cn(X.L. Jia),

Tel: +86 10 51685755, E-mail address: llke@bjtu.edu.cn (L.L. Ke)

1. Introduction

FGMs was a kind of new type non-homogeneous materials, which were originated in the mid-1980s by a group of Japanese scientists [1,2]as thermal barrier materials for aerospace structures and fusion reactors. An FGM is characterized by a continuous and smooth material composition change in one or more dimensions by gradually varying the microstructure from one material to another material with a specific gradient for the optimum distribution of component materials. FGMs offer many advantages including improved stress distribution, enhanced thermal resistance, higher fracture toughness, and reduced stress intensity factors that make them very attractive in many engineering applications [3].

Micro-Electro-Mechanical Systems (MEMS) is a technology that in its most general form can be defined as miniaturized mechanical and electro-mechanical elements that are made using the techniques of micro-fabrication. It usually consists of a central unit that processes data, the microprocessor and several components that interact with the outside such as micro-sensors, see Fig. 1.

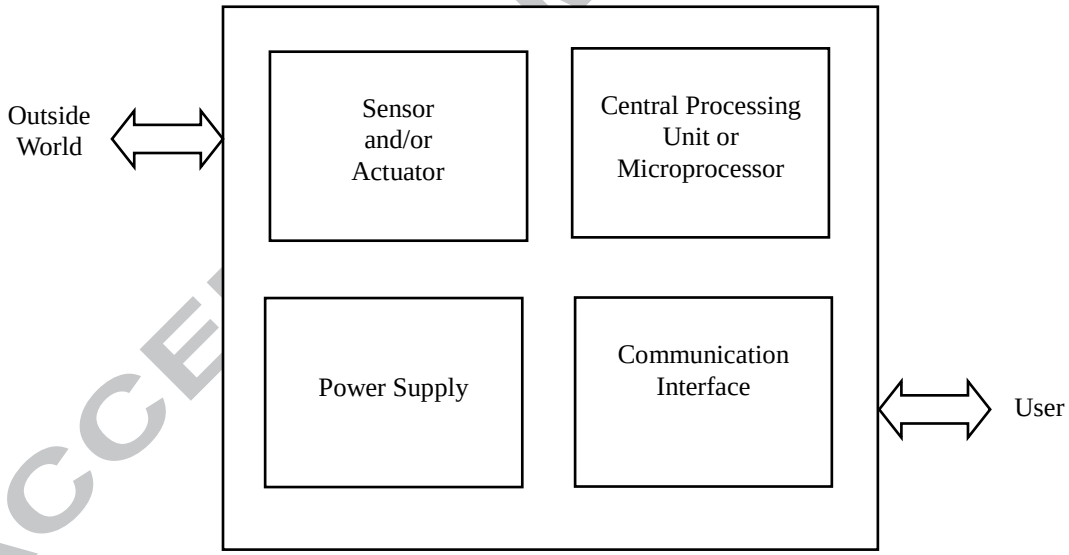

Fig. 1. Components of MEMS.

Most recently, the use of FGMs in MEMS structures has been proposed to solve the problem that it is difficult to meet all material and economical requirements using a single layer process with homogenous materials when integrating MEMS devices on top of the integrated circuit (IC) [4,5], due to their above-mentioned advantages. Especially, Witvrouw and his co-workers [6,7] developed a multilayer poly-SiGe deposition process for fabricating MEMS structural layers in

gyroscope. They found that the ploy-SiGe showed excellent mechanical properties in the MEMS applications.

However, it is noteworthy that the size effect is of importance when apply FGMs in MEMS structures. It is well-known that the classical elasticity theory which does not include an internal material length scale parameter, fails to characterize the size effect phenomenon. Consequently, utilization of higher order theories is necessary, such as the couple stress elasticity [8,9], nonlocal elasticity [10], strain gradient elasticity [11], strain gradient plasticity [12], surface elasticity [13] and modified couple stress theory [13]. Among these higher order theories, the modified couple stress theory proposed by Yang *et al.* [14] has been widely used to study the size-dependent mechanical behavior of micro-scale structures. In this theory, the constitutive equations involve only one additional internal material length scale parameter besides two classical material constants. Recently, this theory has been further employed to establish the size-dependent FGM micro-beam and micro-plate models. Reddy *et al.* [15,16] proposed the microstructure-dependent nonlinear theory for micro plates which accounts for the through-thickness power-law variation of a two-constituent material and size effect. Ke *et al.* [17-20] investigated the bending, buckling and vibration of size-dependent FGM microbeams and annular microplates.

With the further development of aerospace engineering, petroleum exploration environmental inspections and so on, MEMS devices are expected to be used in high extreme industrial temperature environments. Therefore, the properties of FGM MEMS devices under the combined electrostatic force and temperature change need to make an in-depth study. The pull-in instability of FGM MEMS arose from the heat generated by an electric current was discussed by Hasanyan *et al.* [21]. They found that the pull-in voltage can be regulated by varying volume fractions of two constituents through the thickness of an FGM plate. The study by Mohammadi-Alasti *et al.* [22] indicated that a temperature change resulted in the deflection of the cantilever FGM micro-beam due to the variable thermal expansion coefficient along the thickness. Rezaee *et al.* [23] investigated the mechanical behavior of the FGM micro-tweezer under DC voltage and temperature variations. It was found that increasing the ceramic percentage increased the system equivalent stiffness. However, little attention has been done on the two important factors, i.e. geometric nonlinearity and intermolecular force in the above analysis. Based on the von Kármán nonlinear theory, Wang *et al.* [24] discussed the influence of the length scale parameter and Poisson's ratio on the bending and thermal post-buckling behavior of micro-beams. The dynamic response of homogeneous, thermoelastic micro-beam resonators subjected to time-varying transverse loads was investigated in the context of the generalized theory of thermos-elasticity by Sharma *et al.* [25], without considering the size effect. Komijani *et al.* [26] analyzed buckling and

post-buckling and small amplitude vibrations in the pre/post-buckling regimes of functionally graded beams resting on a nonlinear elastic foundation based on the modified couple stress theory. They also investigated the nonlinear dynamic characteristics of functionally graded piezoelectric material beams under in-plane and out-of-plane mechanical, thermal, and electrical excitation [27]. Based on the same theory, thermal buckling and vibration of functionally graded sinusoidal microbeams with temperature-dependent properties and three kinds of temperature distributions are investigated by Lei et al [28]. However, the research by Komijani *et al.* and Lei *et al.* did not involve the thermal-mechanical-electrical coupling effect in MEMS application. Jia *et al.* [29] studied the pull-in instability and free vibration of electrostatically actuated FGM micro-beams in MEMS, allowing for the geometric nonlinearity and intermolecular Casimir force, but without considering the temperature change. Later, they analyzed the thermal effect on the pull-in instability of FGM micro-beams subjected to electric actuation, without considering size-dependent effect [30]. Recently, they investigated the size effect on the free vibration of functionally graded micro-beams under the combined electrostatic force, temperature change and Casimir force based the modified couple stress theory [31].

This paper investigates the thermal-mechanical-electrical buckling of fixed FGM micro-beams under a combined action of electrostatic force, temperature change and Casmir force within the framework of von Kármán nonlinearity and the modified couple stress theory. The temperature-dependency of the effective material properties is specially considered. The nonlinear buckling and thermal buckling results of the micro-beam are obtained by using DQ method. The effects of the volume fraction profile parameter, dimensionless length scale parameter, initial gap ratio, ground electrode shape parameter, the applied voltage, slenderness ratio and the axial residual stress on the thermal-mechanical-electrical buckling behavior are discussed in detail through parametric studies. To the authors' best knowledge, no previous studies which cover all these issues are available.

2. The modified couple stress theory

In this paper, equilibrium of the moment of couples is introduced as an additional equation for the couple stresses. The additional equilibrium relation requires the couple stress tensor to be symmetric. As a result, the only deformation measures, which contribute to the deformation energy, are the symmetric parts of the displacement gradient (strain tensor) and the rotation gradient (symmetric curvature tensor). A linear elastic constitutive law for isotropic couple stress

materials is developed on this basis. The number of material length scale parameters is reduced from the two in the classical couple stress theories to only one in the present theory. The torsion of a thin cylindrical bar and the bending of a thin plate of infinite width are presented to illustrate the effect of the strain gradients in the modified couple stress theory [14].

$$U_s = \frac{1}{2}\int_{\Lambda} \boldsymbol{\sigma} : \boldsymbol{\varepsilon} + \mathbf{m} : \boldsymbol{\chi}\, d\Lambda, \tag{1}$$

in which, the Green small strain tensor $\boldsymbol{\varepsilon}$, stress tensor $\boldsymbol{\sigma}$, the symmetric curvature tensor $\boldsymbol{\chi}$ and the deviatoric part of the couple stress tensor $\mathbf{m}$ are respectively defined as

$$\boldsymbol{\varepsilon} = \frac{1}{2}\left[\nabla \mathbf{u} + \nabla \mathbf{u}^{\mathrm{T}}\right], \tag{2}$$

$$\boldsymbol{\sigma} = \lambda \mathrm{tr}\ \boldsymbol{\varepsilon}\ \mathbf{I} + 2\mu\boldsymbol{\varepsilon}, \tag{3}$$

$$\boldsymbol{\chi} = \frac{1}{2}\left[\nabla \boldsymbol{\Theta} + \nabla \boldsymbol{\Theta}^{\mathrm{T}}\right], \tag{4}$$

$$\mathbf{m} = 2l^2\mu\boldsymbol{\chi}, \tag{5}$$

where $\mathbf{u}$ is the displacement vector, λ and μ are lame's constants. l is a material length scale parameter, which is regards as a material property characterizing the effect of the couple stress. $\boldsymbol{\Theta}$ is the rotation vector expressed as

$$\boldsymbol{\Theta} = \frac{1}{2}\mathrm{curl}\ \mathbf{u}. \tag{6}$$

3. FGM beam model

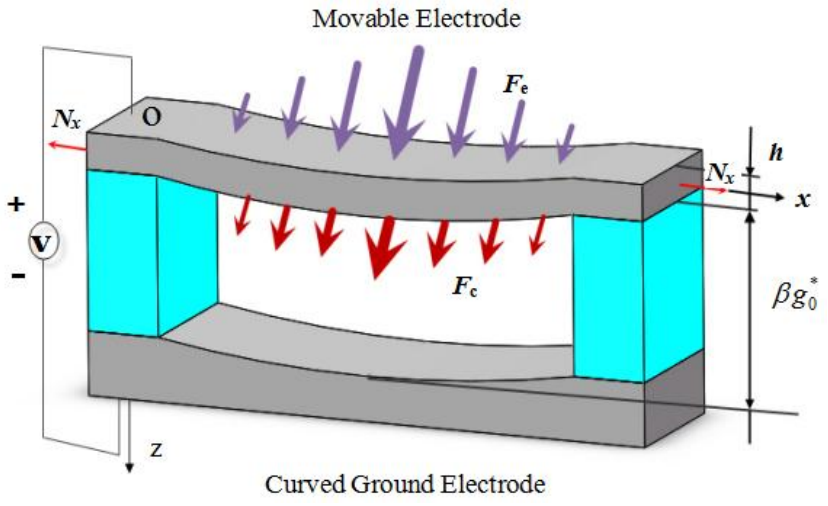

(a)

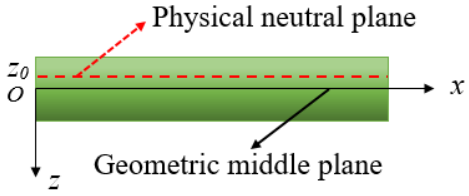

(b)

Fig. 2. A beam model for the MEMS device: (a) Fixed-fixed micro-beam with curved ground electrode ($\beta > 0, \beta \neq 1$); (b) Physical neutral plane and geometric middle plane.

Fig. 2(a) shows the structure of a typical MEMS device, e.g., a micro-resonator and micro-switch, where the key components include a fixed electrode modeled with curved upper face as a ground plane, and a movable upper electrode modeled as a FGM micro-beam with length *L*, width *b*, and thickness *h*, which subjected to axial load, electrostatic force, Casimir force and an uniform temperature change ΔT. The two electrodes are separated by a dielectric spacer with an initial gap $g_0(x)$. The origin of the *x*-coordinate is set as the intersection of the geometric middle plane and the left end of the movable electrode. *w*, *u* denotes the transverse and axial deflections of a point on the physical neutral plane, respectively.

In general, the curved upper face of the ground electrode is assumed to be a symmetrical second-order polynomial shape

$$g_0(x) = g_0^*\left[1+\frac{4(\beta-1)}{L^2}(Lx-x^2)\right], \tag{7}$$

where g_0^* denotes the gap distance at fixed ends $x=0$ and $x=L$, β is the ground electrode shape parameter characterizing the ground electrode shape, βg_0^* represents the initial gap at the middle point $x=L/2$, see Fig. 2(a). The ground electrode surface is convex when $\beta<1$ and concave when $\beta>1$. As a special case $\beta=1$ indicates a flat ground electrode and a uniform initial gap along the beam length.

For the FGM micro beams, the physical neutral plane does not coincide with the geometric middle plane due to the inhomogeneous material properties in the thickness direction, see Fig. 2(b). Eltaher *et al.* investigated the bending, buckling and vibration of FGM nano-beams based on the physical neutral plane and nonlocal theory[32,33]. Ke *et al.* analyzed the axisymmetric postbuckling of functionally graded material annular microplates considering physical neutral plane[20]. Their studies showed that the use of physical neutral plane can eliminate the bending-extension coupling in FGM structures. The z-coordinate of the physical neutral plane z_0 can be expressed as[32,33]

$$z_0 = \frac{\int_{-h/2}^{-h/2} E_f \ z \ z dz}{\int_{-h/2}^{-h/2} E_f \ z \ dz} . \tag{8}$$

in which, E_f is the Young's modulus of the FGM micro-beam.

The deflection of the micro-beam is caused by the electrostatic force induced by an applied voltage, temperature change, intermolecular Casimir force and axial load. The axial load N_x consists of two components, one is due to the residual strain from the fabrication process, denoted by N_a, another is extra axial force N_e, both are positive for a tensile force, and vice versa.

Due to the comprehensive function of above factors, the micro-beam deflects towards the ground electrode under the action of axial force N_x, distributed electrostatic force F_e, Casmir force F_c and thermal strain. Both F_e and F_c are nonlinear functions of the gap $g\ x = g_0\ x - w\ x,t$ between the deformed micro-beam and the ground electrode.

Taking into account the first-order fringing field correction, the electric field force per unit length can be written as

$$F_e = \frac{\varepsilon_0 b V^2}{2\left[g_0\ x - w\ x,t \right]^2} + \frac{0.65\varepsilon_0 V_0^2}{2\left[g_0\ x - w\ x,t \right]} , \tag{9}$$

where $\varepsilon_0 = 8.854\times10^{-12}\ \mathrm{C^2N^{-1}m^{-2}}$ is the permittivity of vacuum. The Casimir force takes the form of [34, 35]

$$F_c = \frac{\pi^2 \bar{h} c b}{240\left[g_0\ x - w\ x,t \right]^4} , \tag{10}$$

in which $\bar{h} = 1.055\times10^{-34}\ \mathrm{Js}$ is Planck's constant divided by 2π, and $c = 3\times10^8\ \mathrm{ms^{-1}}$ is the speed of light.

In this paper, the FGM micro-beam is a mixture of Silicon nitride (Si_3N_4) and Nickel (Ni). Si_3N_4 is material phase 1, whose volume fraction is V_1, and Nickel (Ni) is material phase 2, whose volume fraction is V_2. The mixing ratio changes smoothly and continuously along the thickness direction. The volume fraction of Silicon nitride V_1 and that of Nickel V_2 are given by [36]

$$V_1 + V_2 = 1, \quad V_2(z) = \left(\frac{2z + h}{2h} \right)^n , \tag{11}$$

where the superscript "n" is a power law index that defines the volume fraction profile through beam thickness and can be varied to tailor for desired performance. It is noted that $n = 0$ corresponds to a pure Ni micro-beam. The volume fraction profile is Si_3N_4-rich at the top

beam surface ($z=-h/2$) , whereas Ni -rich at the bottom surface ($z=h/2$).

The effective material properties P_f of the FGM layer, like Young's modulus E_f , Poisson's Ratio ν_f and thermal expansion coefficient α_f can then be obtained base on the Voigt model

$$P_f=\sum_{j=1} P_j V_j \,, \tag{12}$$

where P_j and V_j are the material properties and volume fraction of the constitute material j, and

$$\sum_{j=1} V_j = 1 . \tag{13}$$

Since FGM structures are most commonly used in the high-temperature environment, where significant changes in mechanical properties of the constituent materials are to be expected [37], it is essential to take into consideration this temperature-dependency for accurate prediction of the mechanical response. Thus, the effective material properties P_f can be expressed as a nonlinear function of environment temperature T(K) [38]

$$P_j = P_0 \left(P_{-1}T^{-1}+1+P_1T+P_2T^2+P_3T^3 \right) , \tag{14}$$

where $T=T_0+\Delta T$ and T_0=300K (room temperature), P_0, P_{-1}, P_1, P_2 and P_3 are temperature dependent coefficients and are unique to the constituent materials. From Eqs. (11) and (13), one has the effective Poisson's ratio α_f , coefficient of thermal expansion ν_f, and Young's modulus E_f

$$\alpha_f\left(z, T\right)=\left[\alpha_2 \left(T\right)-\alpha_1 \left(T\right)\right]\left(0.5-\frac{z}{h}\right)^n+\alpha_1 \tag{15}$$

$$\nu_f\left(z, T\right)=\left[\nu_2 \left(T\right)-\nu_1 \left(T\right)\right]\left(0.5-\frac{z}{h}\right)^n+\nu_1 \tag{16}$$

$$E_f\left(z,T\right)=\frac{\left[E_2\left(T\right)-E_1\left(T\right)\right]\left(0.5-\frac{z}{h}\right)^n+E_1}{1-\nu_f^2}. \tag{17}$$

4. Theoretical formulations and solution procedures

4.1 Theoretical formulations

The total strain at the x direction is the sum of the mechanical strain ε_m and thermal strain ε_T , i.e., $\varepsilon_{xx}=\varepsilon_m+\varepsilon_T$. von Karman type nonlinear strain components for micro-beams undergoing moderately large deformation can be denoted as

$$\varepsilon_{xx}=\frac{\partial u}{\partial x}-\left(z-z_0\right)\frac{\partial^2 w}{\partial x^2}+\frac{1}{2}\left(\frac{\partial w}{\partial x}\right)^2, \quad \varepsilon_{yy}=\varepsilon_{zz}=\varepsilon_{xy}=\varepsilon_{xz}=\varepsilon_{yz}=0. \tag{18}$$

and $\varepsilon_T = \alpha_f \ T - T_0 \ = \alpha_f \Delta T$. From Eq.(18), the constitutive relationships of the FGM micro-beam are given as

$$\sigma_{xx} = E_f \left[\frac{\partial u}{\partial x} - \ z - z_0 \ \frac{\partial^2 w}{\partial x^2} + \frac{1}{2}\left(\frac{\partial w}{\partial x} \right)^2 - \alpha_f \Delta T \right], \ \sigma_{yy} = \sigma_{zz} = \sigma_{xy} = \sigma_{xz} = \sigma_{yz} = 0 \quad (19)$$

The rotation vector components can be deduced from Eq.(6),

$$\Theta_y = -\frac{\partial w}{\partial x}, \ \Theta_x = \Theta_z = 0 \quad (20)$$

Substitute Eq. (20) into Eqs. (4) and (5), it obtains

$$\chi_{xy} = -\frac{1}{2}\frac{\partial^2 w}{\partial x^2}, \ \chi_{yy} = \chi_{zz} = \chi_{xy} = \chi_{xz} = \chi_{yz} = 0 \quad (21)$$

$$m_{xy} = -\mu_f l^2 \frac{\partial^2 w}{\partial x^2}, \ m_{yy} = m_{zz} = m_{xy} = m_{xz} = m_{yz} = 0 \quad (22)$$

where $\mu_f = E_f \Big/ \left[2 \ 1 + \nu_f \ \right]$. The strain energy of the micro-beam can be calculated from

$$U_s = \int_\Lambda \int_0^{\varepsilon_m} \sigma_{xx} d\varepsilon_m d\Lambda + \int_\Lambda m_{xy} \chi_{xy} d\Lambda =$$

$$\frac{1}{2}\int_\Lambda E_f \left[\frac{\partial u}{\partial x} - \ z - z_0 \ \frac{\partial^2 w}{\partial x^2} + \frac{1}{2}\left(\frac{\partial w}{\partial x} \right)^2 - \alpha_f \Delta T \right]^2 d\Lambda + \frac{1}{2}\int_\Lambda \mu_f l^2 \left(\frac{\partial^2 w}{\partial x^2} \right)^2 d\Lambda . \quad (23)$$

The total transverse distributed force per unit length $q = F_e + F_c$ is measured positive in the direction of the deflection *w*. Then, the work done by *q* can be stated as

$$W_q = \int_0^L \int_0^w q dw \, dx = \int_0^L \left[\int_0^w \left[\frac{\varepsilon_0 b V^2}{2(g_0 - w)^2} + \frac{0.65\varepsilon_0 V^2}{2(g_0 - w)} + \frac{\pi^2 \bar{h} c b}{240(g_0 - w)^4} \right] dw \right] dx . \quad (24)$$

While the work done by the axial force is

$$W_N = \frac{1}{2}\int_0^L N_x \left(\frac{\partial w}{\partial x} \right)^2 dx . \quad (25)$$

Based on the principle of the minimum total potential energy $\delta \ U_s - W_q - W_N \ = 0$, and setting the coefficients of δw and δu as zero leads to the governing equations

$$J_1 \Delta T - N_x \ \frac{\partial^2 w}{\partial x^2} - k_1 \left[\frac{3}{2}\left(\frac{\partial w}{\partial x} \right)^2 \frac{\partial^2 w}{\partial x^2} + \frac{\partial^2 u}{\partial x^2}\frac{\partial w}{\partial x} + \frac{\partial u}{\partial x}\frac{\partial^2 w}{\partial x^2} \right] + \ k_1 z_0 - k_2 \ \frac{\partial^3 u}{\partial x^3} + k' \frac{\partial^4 w}{\partial x^4} = q, \quad (26)$$

$$k_1 \frac{\partial^2 u}{\partial x^2} + k_1 \frac{\partial w}{\partial x}\frac{\partial^2 w}{\partial x^2} + \ k_1 z_0 - k_2 \ \frac{\partial^3 w}{\partial x^3} = 0, \quad (27)$$

in which,

$$k_1 = \int_{-\frac{h}{2}}^{\frac{h}{2}} \hat{E}_f b dz,\ k_2 = \int_{-\frac{h}{2}}^{\frac{h}{2}} \hat{E}_f b z dz,\ k_3 = \int_{-\frac{h}{2}}^{\frac{h}{2}} \hat{E}_f b z^2 dz\ ,k_4 = \int_{-\frac{h}{2}}^{\frac{h}{2}} \mu_f b dz\ , \tag{28a}$$

$$k' = k_1 z_0^2 - 2k_2 z_0 + k_3 + k_4 l^2\ J_1 = \int_{-\frac{h}{2}}^{\frac{h}{2}} \hat{E}_f \alpha_f b dz. \tag{28b}$$

The associate boundary conditions for fixed beam can be expressed as

$$u=0,\ w=0,\ \ \partial w/\partial x = 0 \qquad \text{at} \quad x=0 \text{ and } L. \tag{29}$$

Noted that for homogenous micro-beam whose Young's modulus is a constant, therefore, $k_2 = 0$, Eqs.(26)-(28) can reduce to the nonlinear governing equations for a homogenous micro-beam.

From Eqs. (26),(27) and boundary conditions (29), the motion equation for an FGM micro-beam subjected to temperature change accounting for the size effect can be derived as

$$\left[k' - \frac{k_2 - k_1 z_0\ ^2}{k_1}\right]\frac{\partial^4 w}{\partial x^4} + \ J_1 \Delta T - N_x\ \frac{\partial^2 w}{\partial x^2} - \frac{\partial^2 w}{\partial x^2}\int_0^L \left[\frac{k_1}{2L}\left(\frac{\partial w}{\partial x}\right)^2 - \frac{k_2 - k_1 z_0}{L}\frac{\partial^2 w}{\partial x^2}\right] dx = q. \tag{30}$$

To facilitate theoretical formulation and for generality of solutions, the following dimensionless quantities are introduced

$$k = k' + \ k_2 - \ k_1 z_0^2 / \ ,\ \psi = \ J_1 \Delta T - N_x\ L^2 / k\ ,\ \ \zeta_1 = k_1 g_{0m}^2 / 2k\ , \tag{31a}$$

$$\zeta_2 = \ k_2 - k_1 z_0\ \ g_{0m} / k\ ,\ \ \ \overline{w} = w / g_{0m}\ ,\ \ \overline{x} = x / L\ . \tag{31b}$$

where the maximum initial gap $g_{0m} = \beta g_0^*$ for $\beta \geq 1$, and $g_{0m} = g_0^*$ for $0 < \beta < 1$. Hence, Eq.(30) can then be rewritten in dimensionless form as

$$\frac{\partial^4 \overline{w}}{\partial \overline{x}^4} + \psi \frac{\partial^2 \overline{w}}{\partial \overline{x}^2} - \frac{\partial^2 \overline{w}}{\partial \overline{x}^2}\int_0^1 \left[\xi_1 \left(\frac{\partial \overline{w}}{\partial \overline{x}}\right)^2 - \xi_2 \frac{\partial^2 \overline{w}}{\partial \overline{x}^2}\right] d\overline{x} = \overline{q}. \tag{32}$$

The dimensionless distributed force is

$$\overline{q}(\overline{x}) = \frac{R_c}{\overline{g}_0(\overline{x}) - \overline{w}^{\ 4}} + \frac{BV^2}{\overline{g}_0(\overline{x}) - \overline{w}^{\ 2}} + f\ \frac{BV^2}{\overline{g}_0(\overline{x}) - \overline{w}}, \tag{33}$$

in which

$$\overline{g}_0(\overline{x}) = \frac{g_0^*}{g_{0m}}\left[1 + 4\ \ \beta - 1\ \ \ \overline{x} - \overline{x}^2\ \ \right], \tag{34}$$

$$R_c = \frac{\pi^2 \overline{h} c b L^4}{240 g_{0m}^5 k}, B = \frac{\varepsilon_0 b L^4}{2 g_{0m}^3 k}, f = 0.65\frac{g_{0m}}{b}. \tag{35}$$

The non-dimensional boundary conditions are $\bar{w}=0,\ d\bar{w}/d\bar{x}=0$ at $\bar{x}=0$ and 1. it is noted that above governing equation based on modified couple stress theory will reduce to the classical micro beam theory if the size effect is suppressed by setting l=0.

4.2 Solution procedures

Eq.(32) and the associated boundary conditions form a nonlinear partial differential equation system whose exact solution is not available. The DQ method is therefore used to solve this nonlinear system numerically. According to the DQM, the dimensionless deflection $\bar{w}\ \bar{x}$ and its derivatives at an arbitrary point $\bar{x}_i$ are approximated by [39]

$$w=\sum_{j=1}^{N} l_j(x) w\ x_j\ , \tag{36}$$

$$\left.\frac{\mathrm{d}^k w}{\mathrm{d}\bar{x}^k}\right|_{\bar{x}=\bar{x}_i} =\sum_{j=1}^{N} C_{ij}^{\ k}\ w\ x_j\ , \tag{37}$$

where N is the total number of sampling points $\bar{x}_i$ unevenly distributed over the domain[40-42]

$$\bar{x}_1=0.0,\ \bar{x}_2=0.001,\ \bar{x}_j=\frac{1}{2}\left[1-\cos\frac{\pi\ \ j-2}{N-3}\right],\ldots\ldots,\ \bar{x}_{N-1}=0.999,\ \bar{x}_N=1.0\,. \tag{38}$$

The weighting coefficients $C_{ij}^{\ k}$ are dependent on the distribution of sampling points only and can be calculated from recursive formulae

$$C_{ij}^{\ 1}=\frac{\hat{L}\ \bar{x}_i}{\bar{x}_i-\bar{x}_j\ \ \hat{L}\ \bar{x}_j} \qquad i,j=1,2,\ldots,N;\ i\neq j, \tag{39}$$

$$C_{ii}^{\ 1}=-\sum_{j=1,\,j\neq i}^{N} C_{ij}^{\ 1} \qquad i=1,2,\ldots,N, \tag{40}$$

$$\hat{L}\ \bar{x}_i=\prod_{j=1}^{N}\ \bar{x}_i-\bar{x}_j \qquad i,j=1,2,\ldots,N;\ i\neq j. \tag{41}$$

The higher-order weighting coefficient can then be obtained as follows

$$C_{ij}^{\ m}=m\left[C_{ij}^{\ 1}C_{ii}^{\ m-1}-\frac{C_{ij}^{\ m-1}}{\bar{x}_i-\bar{x}_j}\right], \tag{42}$$

$$C_{ii}^{\ m}=-\sum_{j=1,\,j\neq i}^{N} C_{ij}^{\ m}\ , \tag{43}$$

for i, j =1,2,…, N; m =2,3,…, N-1.

Applying DQ approximations to the governing equation (32), one has

$$\sum_{j=1}^{N} C_{ij}^{\ 4}\,\bar{w}_j + \psi \sum_{j=1}^{N} C_{ij}^{\ 2}\,\bar{w}_j - \sum_{j=1}^{N} C_{ij}^{\ 2}\,\bar{w}_j \sum_{k=1}^{N} C_{Nk}^{I} - C_{1k}^{I}\left(\xi_1\left(\sum_{j=1}^{N} C_{ij}^{\ 1}\,\bar{w}_j\right)^2 - \xi_2 \sum_{j=1}^{N} C_{ij}^{\ 2}\,\bar{w}_j\right) = \bar{q}_i \tag{44}$$

in which $\mathbf{C}^{\mathbf{I}} = \mathbf{C}^{(\mathbf{1})\ -1}$, and the distributed force per unit length can be expressed as

$$\bar{q}_i = \frac{R_c}{\bar{g}_0(\bar{x}_i) - \bar{w}(\bar{x}_i)^{\ 4}} + \frac{BV_0^{\ 2}}{\bar{g}_0(\bar{x}_i) - \bar{w}(\bar{x}_i)^{\ 2}} + f\,\frac{BV_0^{\ 2}}{\bar{g}_0(\bar{x}_i) - \bar{w}(\bar{x}_i)}. \tag{45}$$

According to the -technique given by Jang [40], the boundary conditions become

$$\bar{w}_1 = 0,\ \sum_{j=1}^{N} C_{2j}^{\ 1}\bar{w}_j = 0,\ \sum_{j=1}^{N} C_{N-1j}^{\ 1}\bar{w}_j = 0,\ \bar{w}_N = 0. \tag{46}$$

It should be noted that discarding the geometrically nonlinear terms in Eqs.(44)-(46) leads to the governing equations without the effect of the geometric nonlinearity.

Denoting the unknown static displacement by $\bar{\mathbf{w}} = \bar{w}_i^{\ \mathbf{T}}$ and the transverse force vector by $\bar{\mathbf{q}} = \bar{q}_i^{\ \mathbf{T}}$, the buckling external axial force N_{eB} and corresponding deflection $\bar{w}_{\mathrm{B}}$ for C-C micro-beams, when exist, can be determined from governing equations, respectively.

Assuming a trial axial force N_e, let $\bar{q}_i = 2\beta + f\beta + 4R_c\ \bar{w}_i + \beta + f\beta + R_c\ \ (i = 1, 2, ...N)$, which is the linear part in the Taylor series expansion of $\bar{q}_i$. Fig. 3 shows the iterative process (1.1)-(1.4):

(1.1) Solve Eqs.(44)-(46) respectively to find $\bar{\mathbf{w}}$, which is taken as the initial value $\bar{\mathbf{w}}^*$ to be used in the 1st round of iteration.

(1.2) Substituting $\bar{\mathbf{w}} = \bar{\mathbf{w}}^*$ into Eq.(45) to obtain a new force vector $\bar{\mathbf{q}}$ and expressing Eqs.(44)-(46) with this updated $\bar{\mathbf{q}}$ in the matrix equation, respectively yields

$$\mathbf{K}_{\mathrm{NL}}\bar{\mathbf{w}} = \bar{\mathbf{q}}. \tag{47}$$

where $\mathbf{K}_{\mathrm{NL}}$ is the nonlinear "stiffness matrix". The solution of Eq.(44) is denoted as $\bar{\mathbf{w}}^{\ 1}$.

(1.3) Update $\bar{\mathbf{w}}^*$ by $\bar{\mathbf{w}}^* = \bar{\mathbf{w}}^{\ 1}$ and repeat step (1.2) to gain a new solution $\bar{\mathbf{w}}^{(2)}$.

(1.4) Repeat step (1.3) until the deflection converges to a prescribed error tolerance

$$\sqrt{\frac{\sum \bar{\mathbf{w}}^{\ k+1} - \bar{\mathbf{w}}^{\ k}\ ^2}{\sum \bar{\mathbf{w}}^{\ k+1}\ ^2}} \le 0.0001. \tag{48}$$

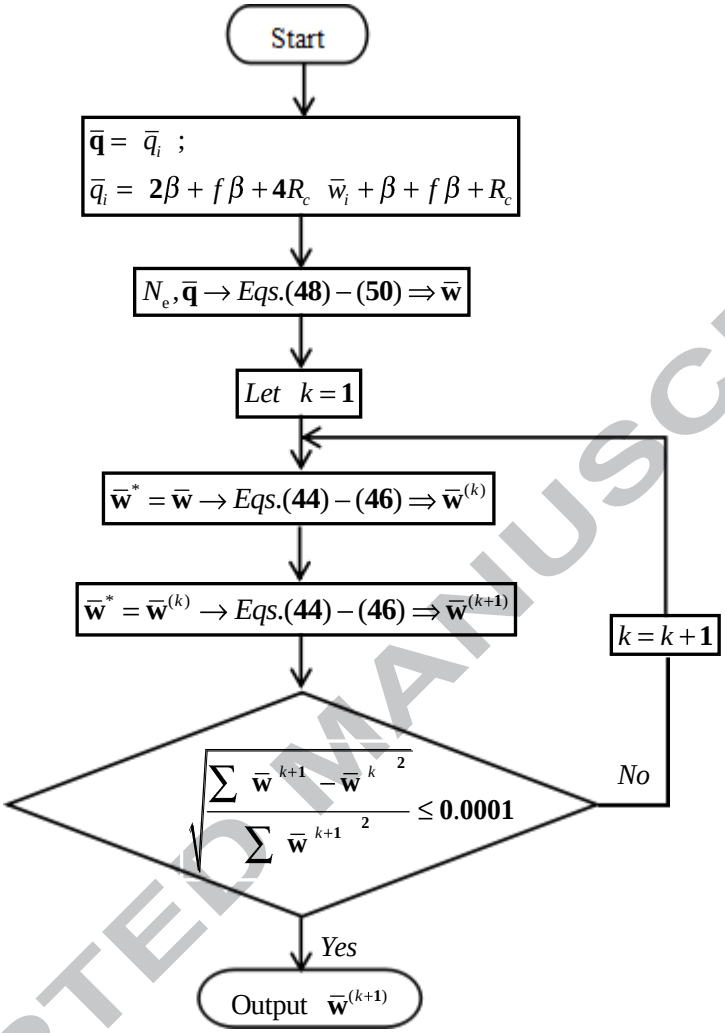

Fig. 3. The flowchart of iterative process.

Increase the axial force N_e and repeat steps (1.1)-(1.4) until the stiffness matrix $\mathbf{K}_{NL}$ becomes singular or the iterative process fails to converge. The last axial force N_e under which the deflection is solvable is the nonlinear external buckling axial force N_{eB}, and the corresponding deflection is the nonlinear buckling deflection $\bar{\mathbf{w}}_B$.

The thermal buckling temperature increment ΔT_B and corresponding deflection $\bar{w}_B$ for fixed micro-beams when exist, are determined using the similar steps above by gradually increasing ΔT.

It should be noted that employing the temperature-dependent material properties in the iterative process, that is using the property values in Eq.(14) by setting $T=T_0+\Delta T$ for a new temperature change, resulted in the temperature-dependent results of the external buckling axial force N_{eB}, thermal buckling temperature variation ΔT_B and corresponding deflection $\bar{w}_B$. While

using the temperature-independent material properties, i.e., the thermo-elastic properties at reference temperature T_0, leaded to the corresponding temperature-independent results.

5. Results and discussions

It should be noted that Table 1 list the material properties of Si_3N_4 and Ni used in this paper. The geometric parameters of the micro-beams are L = 410 μm, b = 100 μm, g_0^* = 1.18 μm, h = 1.5 μm, β=1, the dimensionless material length scale parameter is set to be h/l =10, the axial residual force N_a = 0N, extra axial force N_e = 0N and the ambient temperature T=300K, unless stated otherwise.

Table 1 Temperature-dependent material properties of Si_3N_4 and Ni

Material property	Material	P_0	P_{-1}	P_1	P_2	P_3
Young's Modulus E (P_a)	Si_3N_4	348.43×10^{9}	0	-3.070×10^{-4}	2.160×10^{-7}	-8.946×10^{-11}
	Ni	223.95×10^{9}	0	-2.794×10^{-4}	-3.998×10^{-9}	0
Poisson's Ratio ν	Si_3N_4	0.2400	0	0	0	0
	Ni	0.31	0	0	0	0
Thermal expansion coefficient α (K^{-1})	Si_3N_4	5.8723×10^{-6}	0	9.095×10^{-4}	0	0
	Ni	9.9209×10^{-6}	0	8.705×10^{-4}	0	0

The effective Young's modulus E_f, thermal expansion coefficient α_f, and density ρ_f varying through beam thickness for FGM micro-beams corresponding to different volume fraction profile, i.e. different volume fraction index n. The beam type with n=0 denotes the homogenous micro-beam, and n=1 represents the beam with two phases N_i and Si_3N_4 linear distributed.

To validate the present analysis, the thermal buckling paths of clamped Si_3N_4 micro-beams are compared with the results provided by Komijani et al. [26] in Fig. 4, in which the temperature parameter is defined as $\lambda = \alpha_{ref}\Delta T_B L^2 / 12h^2$, $\bar{w}_{\text{mid}}$ is the deflection of the middle of the beam. From Fig. 4 we can see that both the temperature-dependent(T-dependent) results and the temperature-independent(T-independent) results agree well with the reference [26].

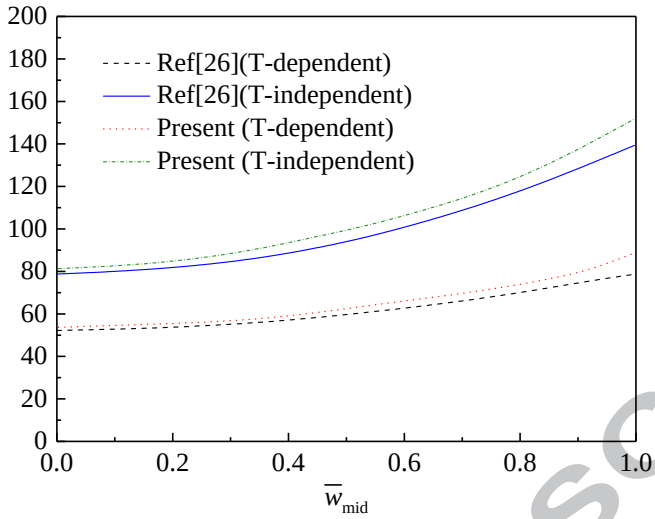

Fig. 4. Thermal buckling paths of clamped Si_3N_4 micro-beams.

5.1 Mechanical-electrical buckling

The effect of the dimensionless length scale parameter h/l on the buckling of the FGM micro-beam is shown in Fig. 5. It could be seen that the nonclassical micro-beam model considering size effect has larger buckling external axial force than the classical beam model because of its high stiffness, and the buckling external axial force N_{eB} increases with the growth of the dimensionless length scale parameter, for both the buckling external axial force N_{eB} calculated from the temperature-dependent analysis and that obtained from the temperature-independent analysis. Besides, it is noted that the temperature-dependent N_{eB} is smaller than the temperature-independent result, however, the difference is not significant with the change of the dimensionless length scale parameter h/l.

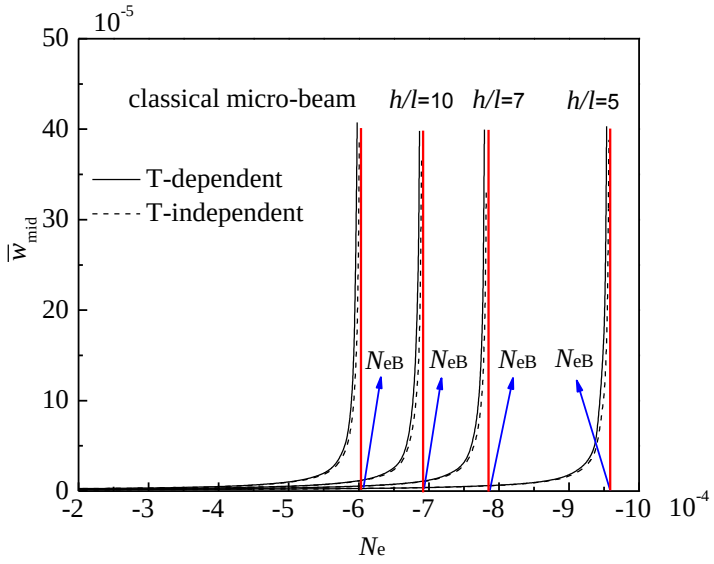

Fig. 5. The effect of the dimensionless length scale parameter h/l on the buckling of the FGM micro-beam.

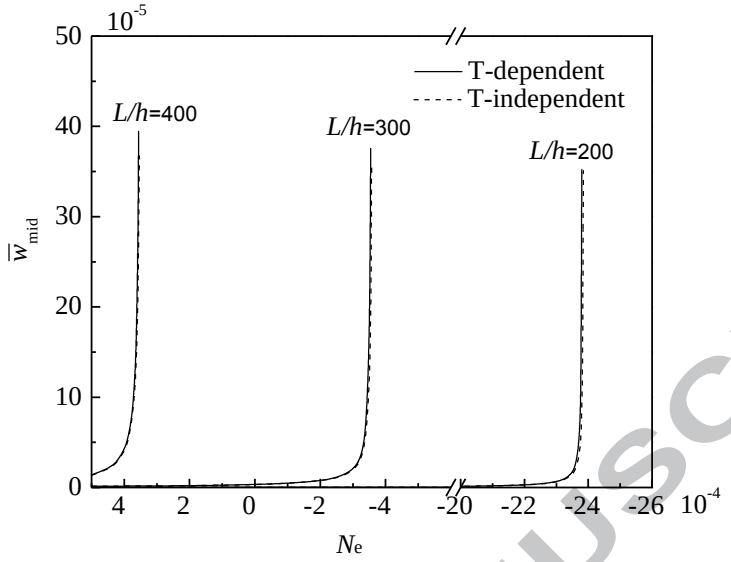

Fig. 6. The effect of the slenderness ratio L/h on the buckling of the FGM micro-beam.

Fig. 6 gives the influence of the slenderness ratio L/h on the buckling of the FGM micro-beams. It shows that the micro-beam with larger slenderness ratio L/h offers a lower buckling external axial force N_{eB}. The temperature-dependent N_{eB} is smaller than the temperature-independent result, but the difference is not significant, and the trend is not change with the decrease of the length scale parameter L/h.

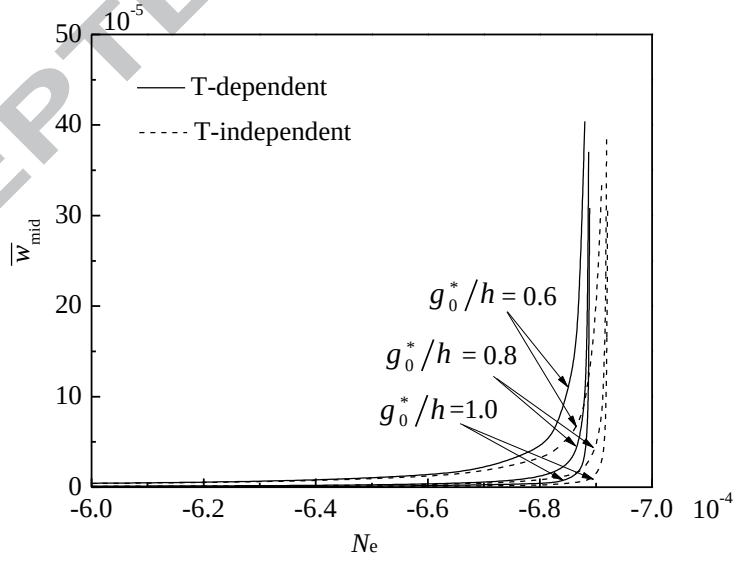

Fig. 7. The effect of the initial gap ratio g_0^*/h on the buckling of the FGM micro-beam.

The influence of the initial gap ratio on the buckling of the FGM micro-beam is shown in Fig. 7. As can be seen that the buckling external axial force N_{eB} increases with the growth of the initial gap ratio. Besides, the temperature-dependent N_{eB} are noticeably smaller than the temperature-independent result especially for larger initial gap ratio.

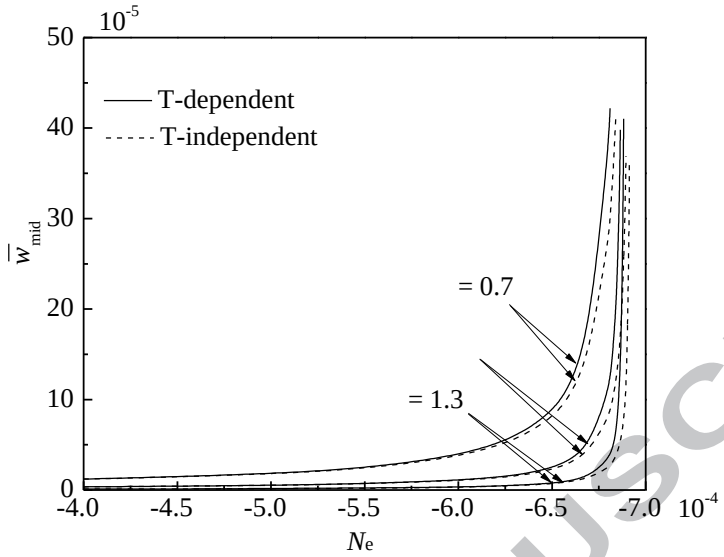

Fig. 8.The effect of the ground electrode shape parameter β on the buckling of the FGM micro-beam.

The buckling of the FGM micro-beam with varying ground electrode shape parameter β are given in Fig. 8. It is noted that with the increase of the external axial force N_e , the deflection of the micro-beam will show a slow growth, then sudden increase when N_e reaches the buckling external axial force N_{eB}. The phenomenon is more obvious for micro-beams with larger ground electrode shape parameter, and the larger ground electrode shape parameter offers a larger buckling external axial force N_{eB}, but the difference is not obvious.

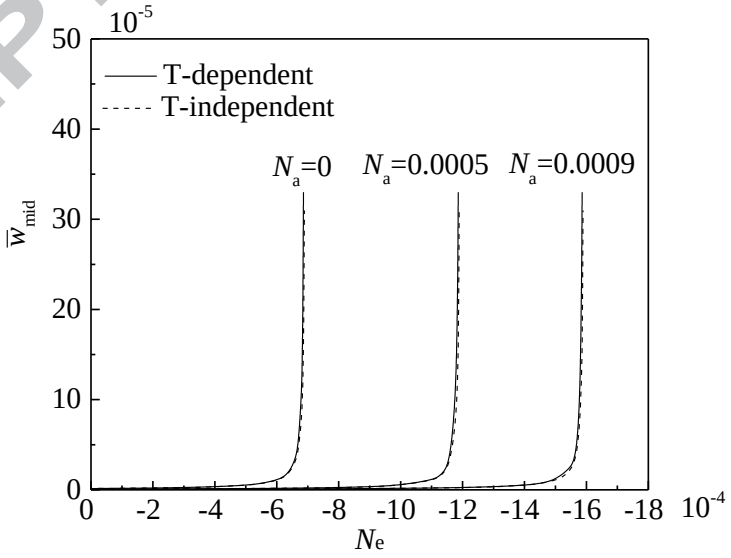

Fig. 9. The effect of the residual axial stress N_a on the buckling of the FGM micro-beam.

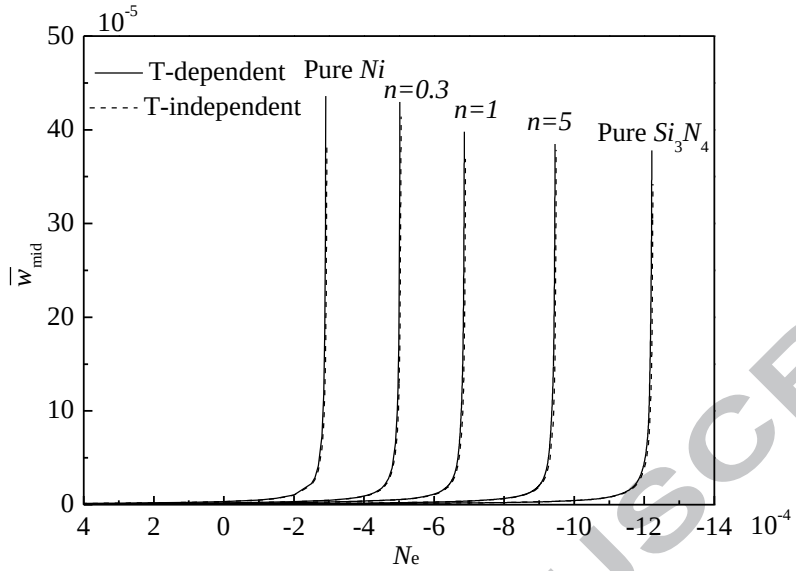

Fig. 10. The effect of the volume fraction index n on the buckling of the FGM micro-beam.

Figs. 9-11 shows the effects of the residual axial stress N_a, the effect of the volume fraction index n and the applied voltage V_0 on the buckling of the FGM micro-beam, respectively. It is noted that the buckling external axial force N_{eB} increases with the growth of the residual axial stress and the volume fraction index, whereas the decrease of applied voltage. Besides, there is a little difference between the temperature-dependent N_{eB} and the temperature-independent result for different residual axial stress N_a, volume fraction index n and the applied voltage V_0.

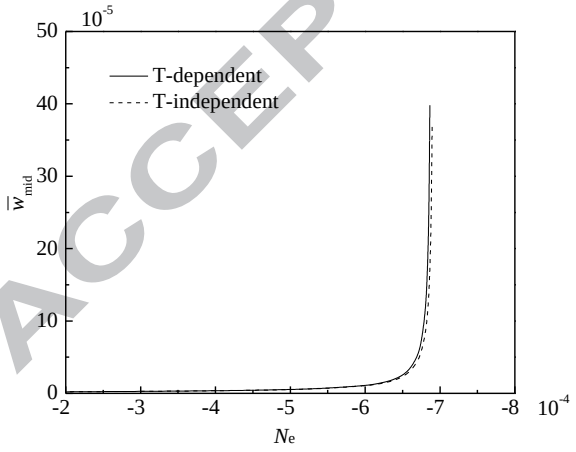

（a）V_0=0V

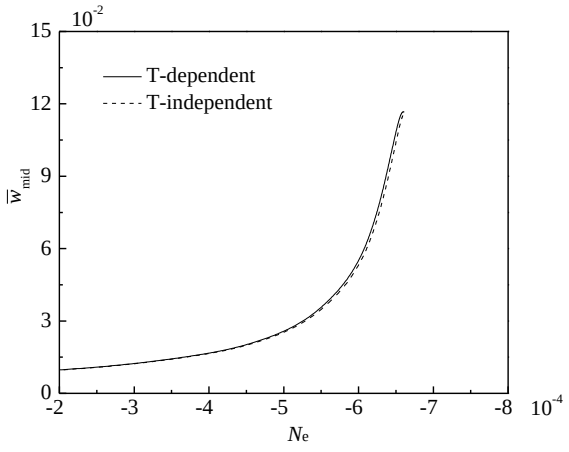

（b）V_0=1V

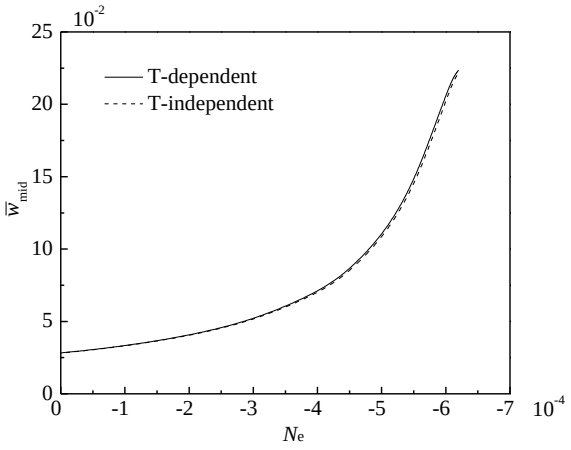

（c）V_0=2V

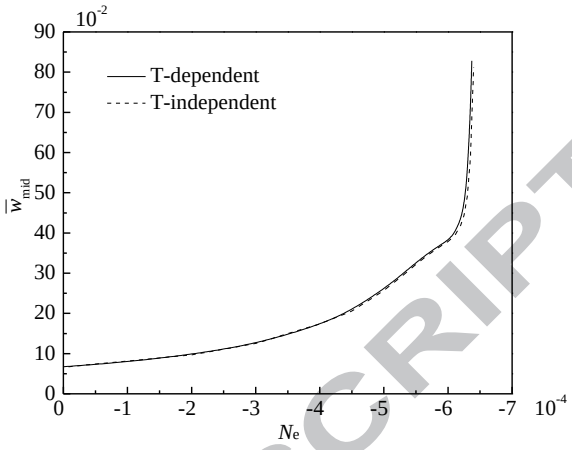

（d）V_0=3V

Fig. 11. The effect of the applied voltage V_0 on the buckling of the FGM micro-beam.

5.2 Thermal-mechanical-electrical buckling

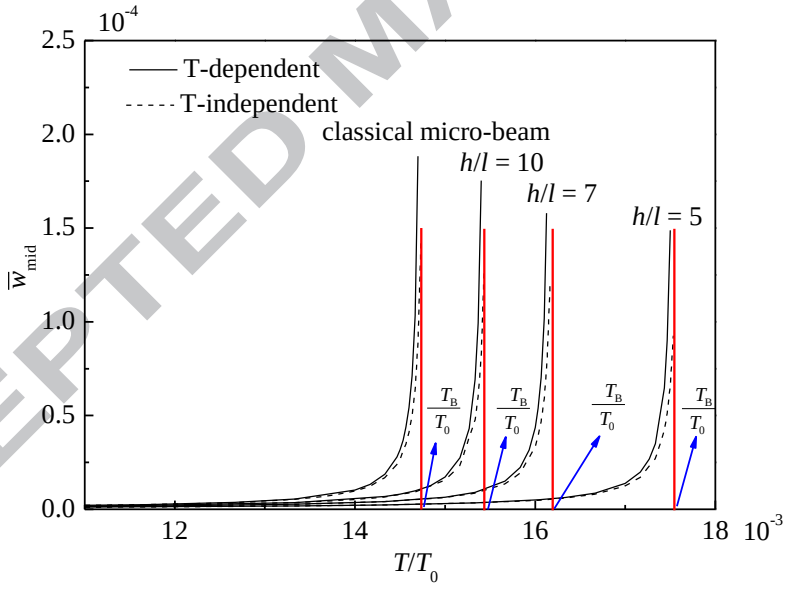

Fig. 12. The effect of the dimensionless length scale parameter *h*/*l* on the thermal buckling of the FGM micro beam.

The effect of the dimensionless length scale parameter *h*/*l* on the thermal buckling of the FGM micro-beam is shown in Fig. 12. It could be seen that the deflection of the micro-beam increase with the growth of the temperature change. The micro-beam will reach a buckling state for a critical temperature increment ΔT_B. the nonclassical micro-beam model considering size effect has larger dimensionless thermal buckling temperature increment ΔT_B than the classical beam model, and the buckling temperature increment ΔT_B increases with the growth of the dimensionless length scale parameter, for both temperature-dependent analysis and temperature-

independent analysis. Besides, it is noted that the temperature-dependent ΔT_{B} is smaller than the temperature-independent result, and the difference increases with the reduction of the dimensionless length scale parameter *h*/*l*.

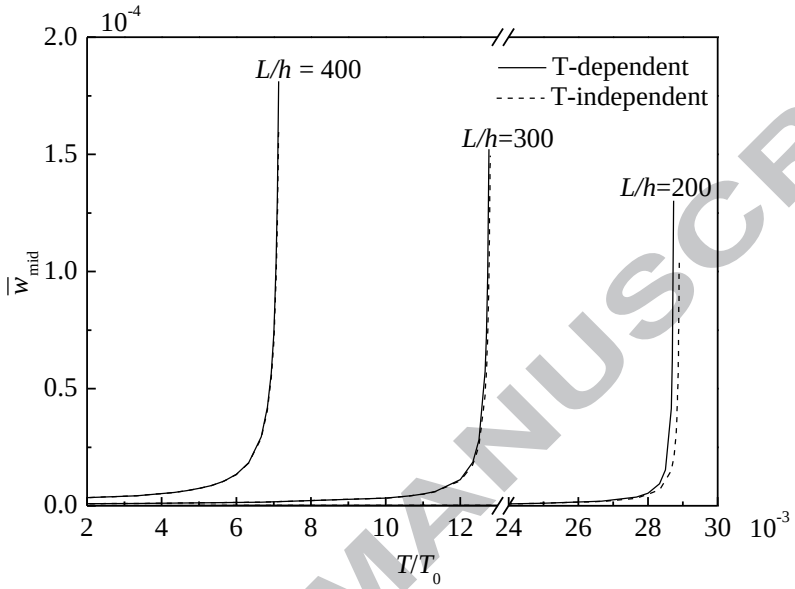

Fig. 13. The effect of the slenderness ratio *L*/*h* on the thermal buckling of the FGM micro beam.

Figs. 13 shows the effects of the slenderness ratio *L*/*h* on the thermal buckling of the FGM micro-beam. It is noted that the dimensionless thermal buckling temperature increment ΔT_{B} increases with the reduction of the slenderness ratio. Besides, the temperature-dependent results are smaller than the temperature-independent result, especially for smaller slenderness ratio *L*/*h*.

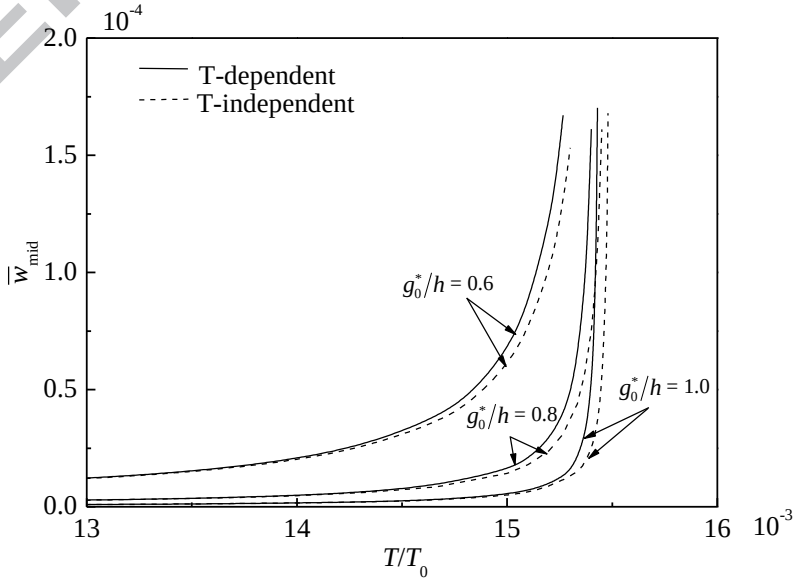

Fig. 14. The effect of the initial gap ratio g_0^*/h on the thermal buckling of the FGM micro beam.

The influences of the initial gap ratio and the ground electrode shape parameter on the

thermal buckling of the FGM micro-beam are shown in Fig. 14 and Fig. 15 respectively. As can be seen that the dimensionless thermal buckling temperature increment ΔT_B increases with the growth of the initial gap ratio and the ground electrode shape parameter. Besides, the temperature-dependent ΔT_B are noticeably smaller than the temperature-independent result especially for larger initial gap ratio and ground electrode shape parameter.

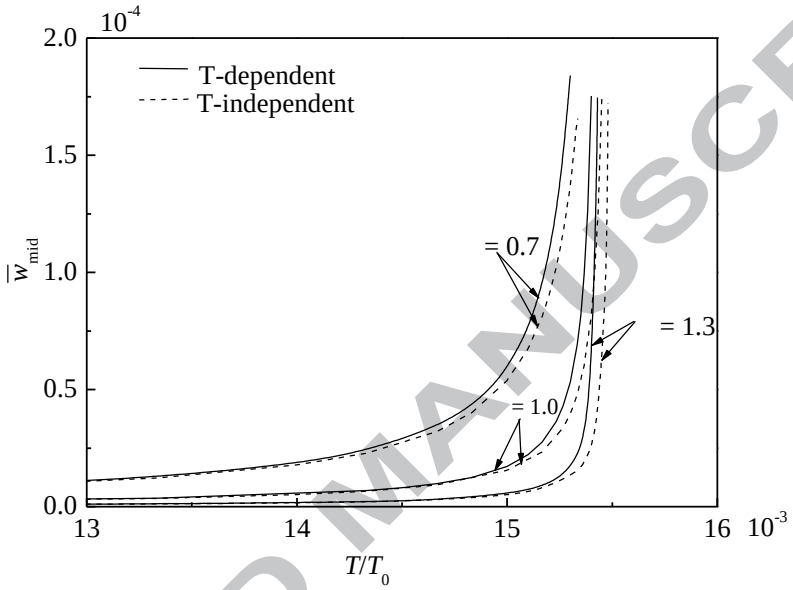

Fig. 15. The effect of the ground electrode shape parameter β on the thermal buckling of the FGM micro beam.

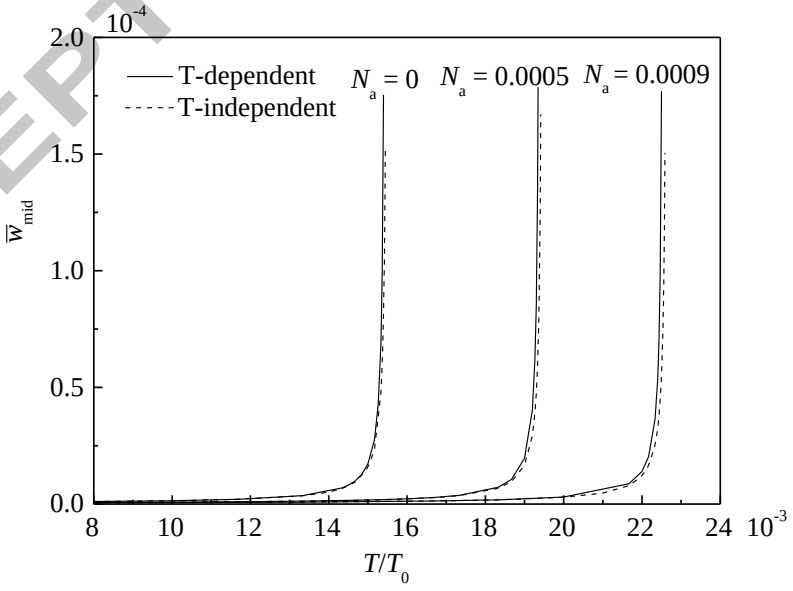

Fig. 16. The effect of the residual tensile stress N_a on the thermal buckling of the FGM micro beam.

Figs. 16-18 shows the effects of the residual axial stress N_a, the effect of the volume fraction index n and the applied voltage V_0 on the thermal buckling of the FGM micro-beam, respectively.

It is noted that the dimensionless thermal buckling temperature increment ΔT_B increases with the growth of the residual axial stress and the volume fraction index, whereas the decrease of applied voltage. Besides, there is a little difference between the dimensionless thermal buckling temperature increment ΔT_{B} and the temperature-independent result for different residual axial stress N_{a}, volume fraction index n and the applied voltage V_0.

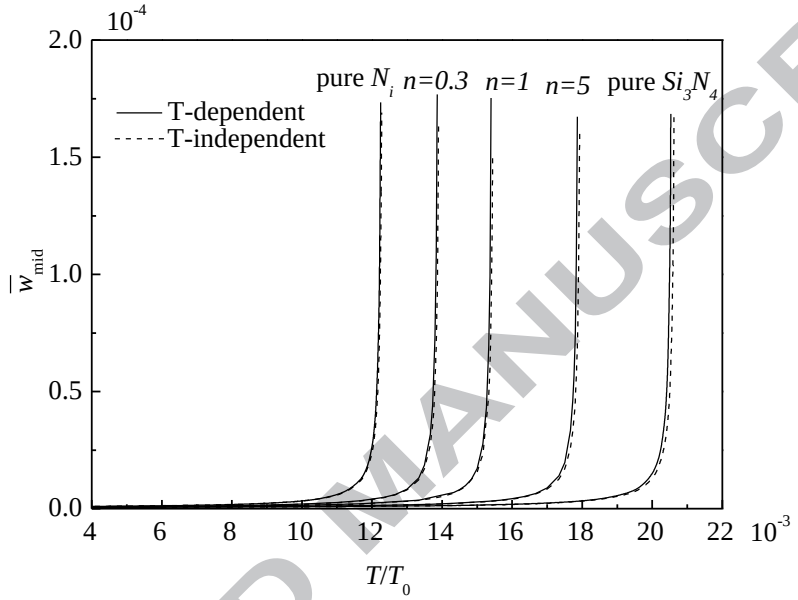

Fig. 17. The effect of the volume fraction index n on the thermal buckling of the FGM micro beam.

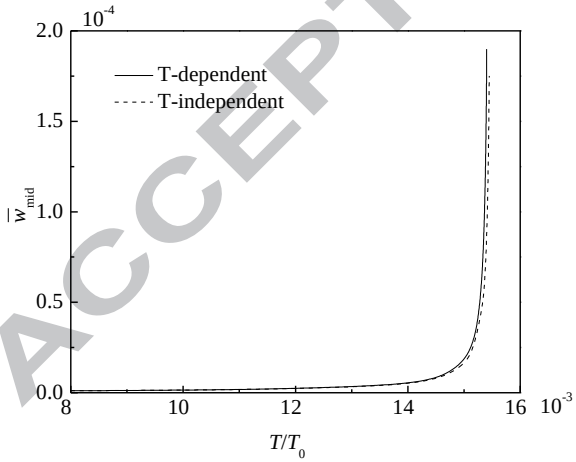

(a) V_0 =0

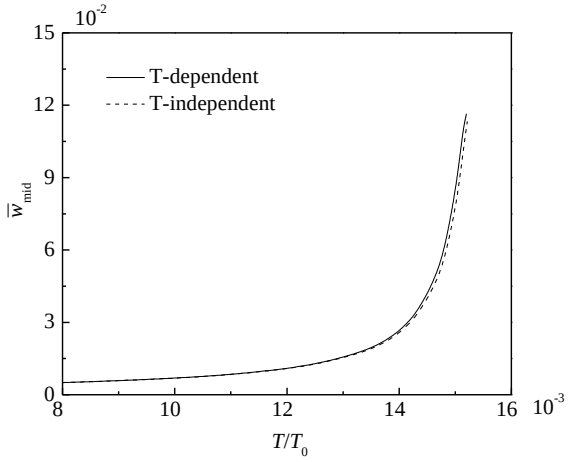

(b) V_0 =1

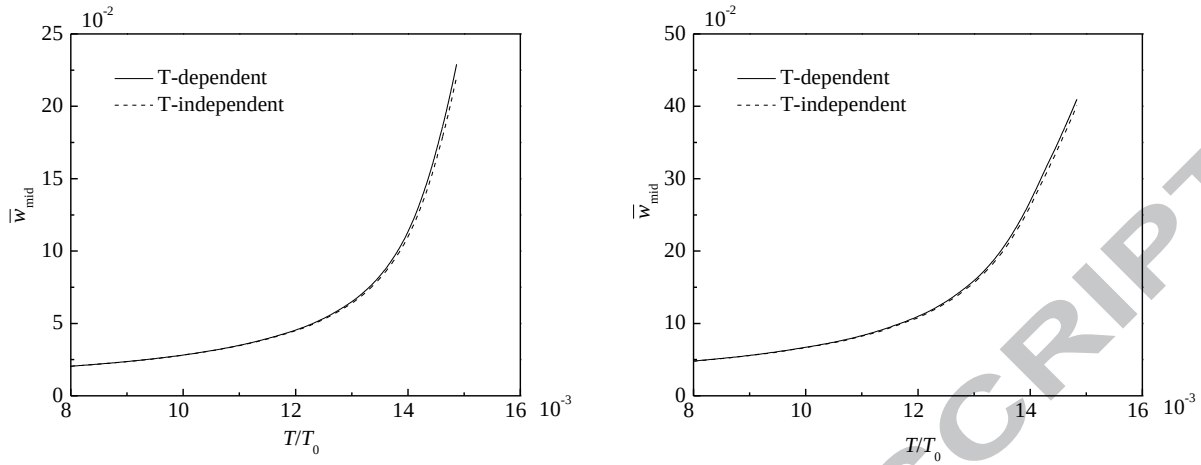

(c) V_0=2 (d) V_0=3

Fig. 18. The effect of the voltage V_0 on the thermal buckling of the FGM micro beam.

5. Conclusions

In this study the modified couple stress theory and von Kármán type geometric nonlinearity are used to investigate the thermal-mechanical-electrical buckling behavior of the functionally graded micro-beams, the temperature-dependency of the effective material properties is specially considered. The governing equation and boundary conditions are derived based on Euler-Bernoulli beam theory, then solved numerically through DQ method. As previously specified, the buckling and thermal buckling properties are influenced differently by material characteristics, geometric dimensions and applied loads. It concluded that: (1) the micro-beam model taking into account the size effect gives the critical buckling external axial force and buckling temperature increment larger than that of the classical micro beam model. (2) the critical buckling external axial force and buckling temperature increment increases with the growth of volume fraction profile parameter, initial gap ratio, axial residual tensile stress and ground electrode shape parameter. (3) the micro-beam with larger dimensionless length scale parameter, applied voltage and slenderness ratio offers a smaller critical buckling external axial force and buckling temperature increment. (4) both the critical buckling external axial force and buckling temperature increment are over-predicted when the temperature dependence of the material properties is not taken into consideration. Furthermore, this discrepancy tends to be much larger with the growth of initial gap ratio and ground electrode shape parameter, and with the decrease of dimensionless length scale parameter h/l and slenderness ratio.

Acknowledgments

The research was financially supported by the National Natural Science Foundation of China (Grant Nos:11402309, 11725207), the National Key Research and Development Plan (Grant No. 2016YFC0303700), the Science Foundation of China University of Petroleum, Beijing(No.2462015YQ0403).

References

[1] Yamanoushi M, Koizumi M, Hiraii T, Shiota I(eds.). Proc 1st Int Symp on Functionally Gradient Materials Japan;1990.

[2] Koizumi M. The concept of FGM. Ceramic Trans 1993; 34:3-10.

[3] Birman V, Byrd LW. Modeling and analysis of functionally graded materials and structures. Appl Mech Rev 2007;60:195-216.

[4] Craciunescu CM, Wuttig M. New ferromagnetic and functionally graded shape memory alloys. J Optoelectron Adv Mater 2003;5:139-46.

[5] Fu YQ, Du HJ, Zhang S. Functionally graded TiN/TiNi shape memory alloy films. Mater Lett 2003;57:2995-9.

[6] Witvrouw A, Mehta A. The use of functionally graded poly-SiGe layers for MEMS applications. Mater Sci Forum 2005;492:255-60.

[7] Gromova M, Mehta A, Baert K, Witvrouw A. Characterization and strain gradient optimization of PECVD poly-SiGe layers for MEMS applications. Sensor Actuat A-Phys 2006; 130:403-10.

[8] Mindlin RD, Tiersten HF. Effects of couple-stresses in linear elasticity. Arch Ration Mech An 1962; 11: 415-48.

[9] Toupin RA. Elastic materials with couple-stresses. Arch Ration Mech An 1962; 11: 385-414.

[10] Eringen AC. Nonlocal polar elastic continua. Int J Eng Sci 1972; 10:1-16.

[11] Aifantis EC. Strain gradient interpretation of size effects. Int J Fracture 1999; 95:1-4.

[12] Hutchinson NA, Hutchinson JW. Strain gradient plasticity. Advances in Applied Mechanics Adv Appl Mech 1997; 33:296-358.

[13] Gurtin ME, Weissmuller J, Larche F. The general theory of curved deformable interfaces in solids at equilibrium. Philos Mag 1998; 178:1093-109.

[14] Yang F, Chong ACM, Lam DCC, Tong P. Couple stress based strain gradient theory for elasticity. Int J Solids Struct 2002; 39:2731-43.

[15] Reddy JN, Berry J. Nonlinear theories of axisymmetric bending of functionally graded circular plates with modified couple stress. Compos Struct 2012; 94:3664-8.

[16] Reddy JN, Kim JS. A nonlinear modified couple stress-based third-order theory of functionally graded plates. Compos Struct 2012; 94: 1128-43.

[17] Ke LL, Wang YS, Yang J, Kitipornchai S. Nonlinear free vibration of size-dependent functionally graded microbeams. Int J Eng Sci 2012; 50:256-67.

[18] Ke LL, Yang J, Kitipornchai S, Bradford MA. Bending, buckling and vibration of size-dependent functionally graded annular microplates. Compos Struct 2012; 94: 3250-7.

[19] Ke LL, Yang J, Kitipornchai S, Bradford MA, Wang YS. Axisymmetric nonlinear free vibration of size-dependent functionally graded annular microplates. Compos Part B-Engineering 2013; 53:207-17.

[20] Ke LL, Yang J, Kitipornchai S, Wang YS. Axisymmetric postbuckling analysis of size-dependent functionally graded annular microplates using the physical neutral plane. Int J Eng Sci 2014; 81: 66-81.

[21] Hasanyan DJ, Batra RC, Harutyunyan S. Pull-in instabilities in functionally graded microthermoelectromechanical systems. J Therm Stresses 2008; 31:1006-21.

[22] Mohammadi-Alasti B, Rezazadeh G, Borgheei AM, Minaei S, Habibifar R. On the mechanical behavior of a functionally graded micro-beam subjected to a thermal moment and nonlinear electrostatic pressure. Compos Struct 2011; 93:1516-25.

[23] Rezaee M, Sharafkhani N, Chitsaz A. Electrostatically actuated FGM micro-tweezer under the thermal moment. Microsyst Technol 2013; 19:1829-37.

[24] Wang YG, Lin WH, Liu N. Nonlinear bending and post-buckling of extensible microscale beams based on modified couple stress theory. Appl Math Modell 2015; 39: 117-27.

[25] Sharma JN, Kaur R. Response of anisotropic thermoelastic micro-beam resonators under dynamic loads. Appl Math Modell 2015; 39:2929-41.

[26] Komijani M, Esfahani SE, Reddy J N, Liu YP, Eslami MR. Nonlinear thermal stability and vibration of pre/post-buckled temperature- and microstructure-dependent functionally graded beams resting on elastic foundation. Compos Struct 2014; 112: 292-307.

[27] Komijani M, Gracie R. Nonlinear thermo-electro-mechanical dynamic behaviour of FGPM beams. Compos Struct 2016; 150:208-18.

[28] Lei J, He YM, Guo S, Li ZK, Liu DB. Thermal buckling and vibration of functionally graded sinusoidal microbeams incorporating nonlinear temperature distribution using DQM. J Therm Stresses 2017; 40:665-89.

[29] Jia XL, Yang J, Kitipornchai S, Lim CW. Pull-in instability and free vibration of electrically

actuated poly-SiGe graded micro-beams with a curved ground electrode. Appl Math Modell 2012; 36:1875-84.

[30] Jia XL, Zhang SM, Ke LL, Yang J, Kitipornchai S. Thermal effect on the pull-in instability of functionally graded micro-beams subjected to electrical actuation. Compos Struct 2014; 116: 136-46.

[31] Jia XL, Ke LL, Feng CB, Yang J, Kitipornchai S. Size effect on the free vibration of geometrically nonlinear functionally graded micro-beams under electrical actuation and temperature change. Compos Struct 2015; 133:1137-48.

[32] Eltaher MA, Alshorbagy AE, Mahmoud FF. Determination of neutral axis position and its effect on natural frequencies of functionally graded macro/nanobeams. Compos Struct 2013; 99:193-201.

[33] Eltaher MA, Khairy A, Sadoun AM, Omar FA. Static and buckling analysis of functionally graded Timoshenko nanobeams. Appl Math Comput 2014; 229:283-95.

[34] Lamoreaux SK. The Casimir force: background, experiments, and applications, Rep Prog Phys 2005; 68: 201-36.

[35] Ganguly P, Desiraju GR. Van der Waals and polar intermolecular contact distances: Quantifying supramolecular synthons. Asian J Chem 2008; 3:868-80.

[36] Reddy JN. Analysis of functionally graded plates. Int J Numer Meth Eng 2008; 47:663-84.

[37] Reddy JN, Chin CD. Thermoelastical analysis of functionally graded cylinders and plates. J Therm Stresses 1998; 21:593-626.

[38] Touloukian YS. Thermophysical properties of high temperature solid materials. McMillan; 1967.

[39] Shu C. Differential quadrature and its application in engineering. Springer-Verlag London Limited; 2000.

[40] Jang SK. Application of differential quadrature to the analysis of structural components, [PhD thesis]. USA: University of Oklahoma; 1987.

[41] Wang X, Bert CW, Striz AG. Differential quadrature analysis of deflection, buckling and free vibration of beams and rectangular plates. Compos Struct 1993; 48:473-9.

[42] Liu GR, Wu TY. Vibration analysis of beams using the generalized differential quadrature rule and domain decomposition. J Sound Vib 2001; 246:461-81.